Abrasion Studies of Nylon 6/Montmorillonite Nanocomposites Using Scanning Electron Microscopy, Fourier Transform Infrared Spectroscopy, and X-ray Photoelectron Spectroscopy

Qi Zhou, Kean Wang, Leslie S. Loo

School of Chemical and Biomedical Engineering, Nanyang Technological University, Singapore 637459, Singapore

Received 18 August 2008; accepted 12 February 2009
DOI 10.1002/app.30229
Published online 7 May 2009 in Wiley InterScience (www.interscience.wiley.com).

ABSTRACT: In this article, abrasion performance of commercial nylon 6 and nylon 6/montmorillonite (MMT) nanocomposites was studied. The polymer nanocomposites showed poor abrasion resistance compared to the neat polymer. The wear loss increased linearly with clay concentration. Changes in surface morphology, composition, and structure were investigated by scanning electron microscopy (SEM), Fourier transform infrared (FTIR)-attenuated total reflection spectroscopy, and X-ray photoelectron spectroscopy (XPS). SEM images showed that all the abraded surfaces contained fractured particles. However, the abraded nanocomposite surfaces had much deeper grooves compared to the homopolymer. FTIR results showed an increase in the amount of α crystals and a decrease in the amount of γ crystals on all the surfaces after abrasion. This was attributed to the strain-induced γ to α crystal transformation. The largest amount of α crystals was formed in the abraded surface of pure nylon 6, and the amount of α crystals formed decreased with increasing MMT content. XPS results showed an increase in the [Si]/[N] elemental ratio for all nanocomposites after abrasion, indicating an increase in the clay content of the surface. Abrasive wear mechanism is as follows: (1) tensile tearing is the dominant wear mechanism for all the samples; (2) the cutting mechanism becomes more important when MMT content increases; (3) the polymer matrix is easier to be removed than clay during the abrasion process; (4) in nylon 6/MMT systems, the poor abrasion resistance is attributed to defects at the clay-polymer interface, resulting in greater wear of the polymer matrix. J Appl Polym Sci 113: 3286–3293, 2009

Key words: nylon 6; clay; nanocomposite; abrasion; surface; crystalline phase transformation

INTRODUCTION

Abrasion resistance is a system property for polymeric materials. The abrasion performance of a given sample is influenced by wear mechanisms involved, abrasive test method utilized, bulk and surface properties of the sample, etc. Lancaster[1] studied the physical processes involved in abrasive wear of a wide range of polymers including nylon. Their results demonstrated that two extreme types of abrasive wear could occur with polymers: (1) cutting, which is caused by relatively sharp asperities and which occurs frequently in more plastic polymers; (2) fatigue, or sometimes tensile tearing, which is caused by more rounded asperities and which tends to be a characteristic of more elastic polymers. These wear mechanisms are, by and large, controlled by the bulk properties of the polymer. Thus Lancaster was able to obtain certain relationships between the wear rate of a polymer with its hardness, tensile strength, and elongation to failure in tensile tests. A number of models that attempted to relate the abrasion resistance of polymers to other mechanical properties have been proposed.[2,3] One of the earliest of these is commonly known as the Ratner–Lancaster correlation, which was found to be suitable for correlating the wear behavior and the mechanical properties of polymers and polymer composites by other authors.[4–7] This model was initially adopted in an extensive way by Ratner and coworkers[8,9] and had been critically reviewed and extended by Lancaster.[1,10] In this theory, three stages are proposed to be involved in the abrasion wear process of polymers: (1) deformation of the surfaces to an area of contact determined by the indentation hardness, H; (2) relative motion opposed by the frictional force, $F = k\mu$; and (3) disruption of material at the contact points involving an amount of work equal to the integral of the stress–strain relationship. An approximate measure of the latter is the product of the

Correspondence to: L. S. Loo (SSLoo@ntu.edu.sg).
Contract grant sponsor: Ministry of Education, Singapore.

stress to break, σ_b, and the elongation to break, ε_b. Thus, the wear rate of a polymer, W, is given by:

$$W = \frac{k\mu}{H\sigma_b\varepsilon_b}, \quad (1)$$

where k is the load, μ is the coefficient of friction, and H is the hardness.

Another important aspect is the effect of fillers on the abrasion performance of polymeric materials. Incorporation of fillers in most polymer composites was found to affect the abrasive wear resistance severely. The filler material can be traditional microscale particles such as glass fiber, carbon fiber, or another polymer with relatively higher abrasive resistance. In recent years, nanoscale fillers were widely incorporated into polymers to produce polymer nanocomposites. Regardless of the filler size, however, the effects of fillers in polymers were found to be beneficial for some materials under certain wear conditions while detrimental for others.[1,2,7,11–13] Bauer and Mehnert[13] did a series of investigations on polyacrylate/SiO_2 nanoparticle coatings, which showed improved scratch and abrasive resistance compared to the neat polymer. On the other hand, fibrillar silicate/styrene-butadiene rubber nanocomposites showed increased wear when the filler content was increased.[11] In general, the abrasion resistance of polymer nanocomposites will be affected by amount of filler added, filler–matrix interaction, and type of matrix. Furthermore, the filler will also change the mechanical properties of polymer matrix, such as increasing the strength and stiffness, while causing corresponding reductions in the elongation to break and ductility.[14–16] Consequently, the effects of fillers on the abrasion resistance of polymer nanocomposites are quite complicated to analyze and predict. In this article, the authors study the effects of montmorillonite (MMT) nanoclay on the abrasion performance of nylon 6.

Nylon 6 has been widely used as engineering plastics in applications such as bearings or packaging materials. Its abrasion resistance is an important property for its widespread applications. Nylon 6/montmorillonite nanocomposites were first successfully synthesized by Toyota research group in the early 1990s. The resulting nanocomposites had excellent mechanical, thermal, and barrier properties. The yield strength and tensile modulus of the nanocomposites increased with nanoclay concentration.[16] However, nylon 6/MMT nanocomposites had poor abrasion performance. Srinath and Gnanamoorthy[7,17] reported the abrasive wear characteristics of melt intercalated nylon 6 nanocomposites, containing 1, 3, and 5 wt % modified MMT clay, using a pin-on-disc abrasion machine. All the nanocomposites they investigated exhibited low abrasive resistance compared to pure nylon.

Generally, the abrasion surfaces are often characterized by scanning electron microscopy (SEM) or microscopy to show their morphology. However, electron microscopy methods are not capable of detecting compositional and structural changes at the abrasion surface. The knowledge of such changes will enable researchers to better understand the micromechanics of the abrasion process and to determine the role played by the nanofillers. This, in turn, will lead to the intelligent design of surfaces with improved abrasion resistance. Spectroscopic techniques such as Fourier transform infrared (FTIR) spectroscopy and Raman are useful for characterizing surface chemical structures.[18] Furthermore, FTIR has been used to investigate the deformation behavior of montmorillonite in nylon 6 nanocomposites.[19] Recently, Raman spectroscopy has also been successfully applied to explain the wear behavior for sintered and thermoplastic polyimides.[20] X-ray photoelectron spectroscopy (XPS) can be used to determine the elemental composition of surfaces.[21] This technique is particularly useful because SEM images do not allow one to distinguish between the nanosized clay platelets and the nylon matrix and also do not provide quantitative information of the various phases on the surface. The purpose of this article is to use FTIR-attenuated total reflectance (ATR) and XPS to investigate the surfaces of nylon 6 and nylon 6/MMT nanocomposites and to study the effects of nanoclay on the abrasive resistance of the nanocomposites. To the authors' knowledge, this is the first time that FTIR and XPS techniques are used to characterize abrasion surfaces.

MATERIALS AND METHODS

Materials

Pure nylon 6 films and nylon 6/montmorillonite nanocomposite films containing 2, 4, 6, and 8 wt % nanoclay were purchased from Nanocor Corporation (Arlington Heights, IL) and used as received. The nanocomposites were made by *in situ* polymerization of nylon 6 with 12-aminododecanoic acid-modified montmorillonite and then melt extruded. The thickness of the films ranged from 0.06 to 0.08 mm.

WAXS measurement

The films were characterized by wide-angle X-ray scattering (WAXS). WAXS was performed on a Rigaku Rint 2000 unit by using Cu Kα radiation at a voltage of 40 kV and a current of 40 mA. The scan speed was 1.0°/min and the scan step was 0.02°.

Abrasion test

Abrasion tests were performed on a Taber model 5135 Abraser under atmospheric conditions (23°C, 55% relative humidity). The films were mounted onto the specimen holder of the Abraser. Two CS-17 Calibrase abrasion wheels were then attached to the Abraser's rollers and the loading was set at 1000 g. CS-17 wheels are resilient wheels that are composed of rubber and aluminum oxide abrasive particles. One thousand cycles were performed on each sample after which the final weight of the sample was measured again. The weight loss during this process was evaluated as the abrasion resistance. Three separated films were tested at each nanoclay concentration, and the results were then averaged.

Scanning electron microscopy

The morphology of abraded surfaces were analyzed by JEOL JSM-6390LA analytical SEM by using an acceleration voltage of 10 keV.

Infrared measurement

FTIR-ATR measurements were performed on the unabraded and abraded surfaces by a Nicolet Nexus 5700 spectrometer by using the Smart Orbit ATR accessory. The Smart Orbit is a high-performance diamond single-reflection ATR. The depth of penetration is ~ 1.5 μm at 1000 cm^{-1} wavelength. The beam splitter is KBr and the detector is a liquid nitrogen-cooled MCT detector. Sixty-four scans were collected for each spectrum at a resolution of 2 cm^{-1}. ATR correction was applied to each spectrum. To determine peak intensities in the region between 900 and 940 cm^{-1}, these spectra were baseline corrected manually. A flat baseline was drawn from 900 and 940 cm^{-1}. Least-squares peak fitting by using Gaussian band shapes was performed by OriginPro 8 software. The peak centers and line widths were not fixed initially.

X-ray photoelectron spectroscopy measurement

XPS measurements were made by using a Kratos Ultra XPS system equipped with an Al $K\alpha_{1,2}$ X-ray source ($h\nu = 1486.6$ eV). The pressure in the analysis chamber was maintained at or below 3.0×10^{-9} Torr during the measurements. The spectra were obtained at a photoelectron takeoff angle of 90° measured with respect to the plane of the sample surface. Peak fitting was performed by using a Shirley baseline. The areas of the XPS peaks were divided by the instrument relative sensitivity factor to account for the different photoionization cross-sections.

RESULTS AND DISCUSSION

Crystal structure and morphology of nylon 6 and nylon 6/MMT nanocomposites

Nylon 6 exhibits polymorphism, and the polymorph depends on the crystallization conditions. At room temperature two crystalline modifications exist, namely the α phase and γ phase.[22,23] The α crystalline phase has a monoclinic structure with crystal parameters $a = 0.956$ nm, $b = 1.724$ nm, $c = 0.801$ nm, and $\beta = 67.5°$.[24] The γ phase also has a monoclinic structure with $a = 0.933$ nm, $b = 1.688$ nm, $c = 0.478$ nm, and $\beta = 121°$.[25] Figure 1 shows the WAXS data for the nylon 6 and nanocomposites films. Only two peaks located at 11° and 21.5° are observed for all specimens. These peaks are attributed to the (020) and (200) planes, respectively, of the γ crystals. No peaks corresponding to the α crystals at $2\theta = 20°$ and $2\theta = 24°$ are seen.[16,26] It can be concluded that the dominant crystalline structure for all the films is the γ phase.

The WAXS region for 2θ less than 10° is usually used to characterize the degree of dispersion of MMT nanoclay: the absence of peaks in this region implies that the nanoclay is fully exfoliated, while the presence of peaks indicates that the clay is intercalated or aggregated.[15] Figure 1 shows that there are no peaks in this region for all the samples, indicating that the MMT clays are fully exfoliated in the nanocomposites.

Abrasion results

Figure 2 shows the abrasion results for the nylon 6 and nanocomposites films. It is observed that the weight loss increases almost linearly with MMT

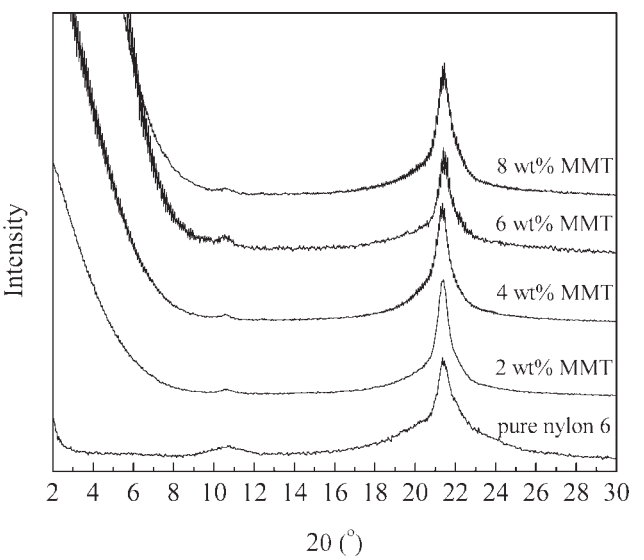

Figure 1 WAXS patterns of pure nylon 6 and nylon 6/MMT nanocomposites.

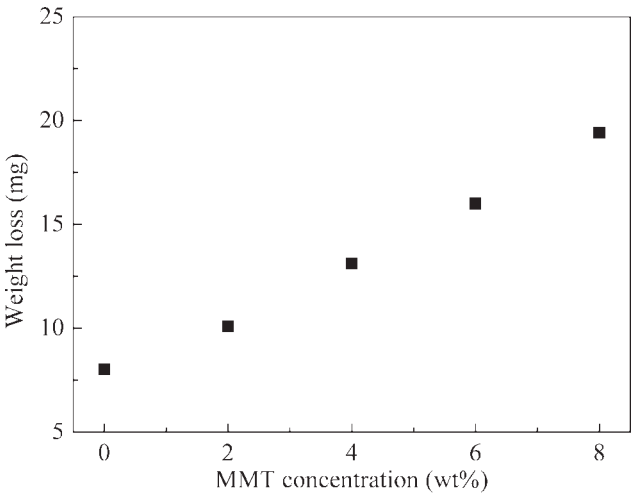

Figure 2 Abrasion weight loss of nylon 6 and nylon 6/nanoclay nanocomposites versus clay content.

content. The lowest loss is incurred by pure nylon 6 films (8.03 mg) and the highest loss is incurred by 8 wt % nanocomposite films (19.4 mg). It is apparent that the presence of MMT in the polymer matrix reduces the abrasion resistance of nylon 6. These results are quite consistent with those obtained by Srinath and Gnanamoorthy,[7,17] as discussed earlier.

SEM results

Figure 3 shows the SEM micrographs of pure nylon 6 and nanocomposites containing 4 and 8 wt % MMT after the abrasion test. Two kinds of deformation are observed here: (1) fractured particles turned up due to the tractive stress and (2) grooves that show the tracks of abrasive particles and are due to the cutting function. The abrasion surface of pure nylon 6 has homogeneously distributed fractured particles and less obvious grooves. However, the wear damage is more serious for the nanocomposites, especially the one with 8 wt % MMT content. As shown in the figure, the abrasion surface of this nanocomposite does not have as many fractured particles but deeper grooves are present. It is observed that the abraded surface of the nanocomposite containing 4 wt % clay contains both fractured particles and grooves. Hence as the MMT content increases, the surface morphology after abrasion contains deeper grooves and less fractured particles.

Crystalline transformation observed by FTIR-ATR

The FTIR spectra and peak assignments of nylon 6 have been published in several articles.[27,28] Figures 4–6 show the ATR spectra of the nylon 6 films. In these spectra, the peak intensities are shown to scale and are displaced vertically relative to each other for clarity of presentation. The spectra before and after the abrasion test were recorded. Figure 4 shows the ATR spectra of the surfaces of pure nylon 6 and nanocomposites containing 4 and 8 wt % MMT nanocomposites in the NH stretching region. It is observed in all the samples that before abrasion, the NH stretching peak is located at around 3282 cm^{-1}, corresponding to the γ crystal phase.[29] However, after abrasion, all the peaks underwent a left shift toward the lower energy region around 3293 cm^{-1}, which is where the NH stretching band for the α

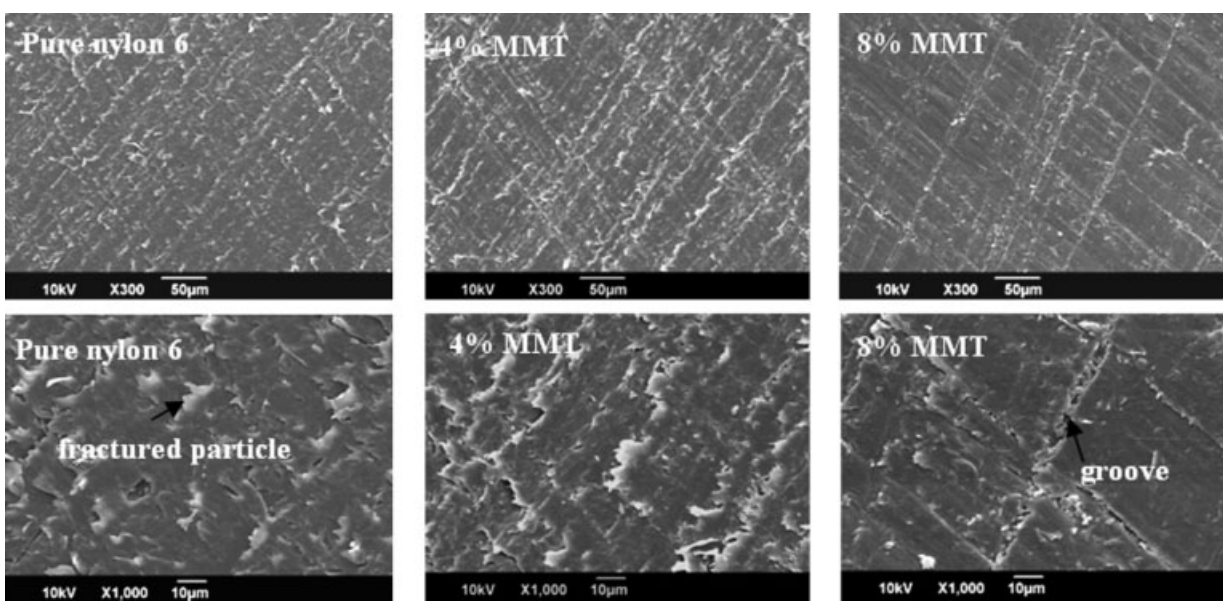

Figure 3 SEM micrographs of the abrasion surfaces of nylon 6 as well as nylon 6 nanocomposites containing 4 wt % MMT and 8 wt % MMT. Top images show magnification at ×300 and bottom images show magnification at ×1000.

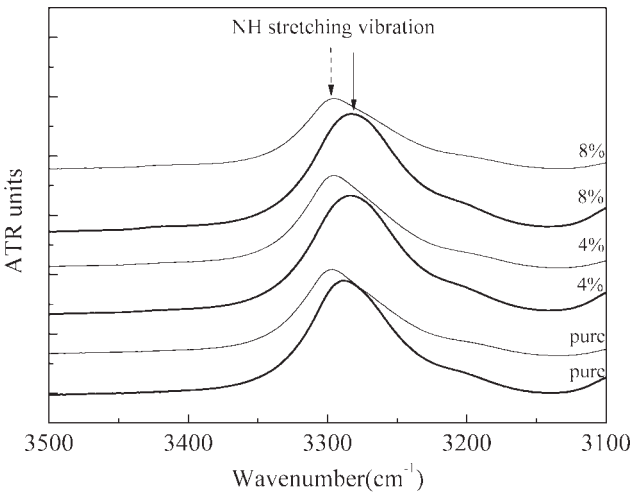

Figure 4 ATR spectra of the N—H stretching region for pure nylon 6 and nylon 6 nanocomoposites containing 4 and 8 wt % MMT before (thick solid lines) and after (thin solid lines) abrasion test.

phase is located.[30] This band shift is attributed to the formation of more α phase crystals at the film surface during abrasion.[31]

More concrete evidence of the increase in the amount of the α crystals at the abrasion surface is given at the lower wavenumber regions of the ATR spectra. Figure 5 shows the ATR spectra of the unabraded and abraded surfaces of pure nylon 6 and nanocomposites containing 4 and 8 wt % MMT nanocomposites in the 1400–1500 cm^{-1} region. In this region, due to the CH_2 scissors deformation, γ crystals have two characteristic peaks at 1463 and 1436 cm^{-1}, while α crystals produce two peaks at 1477 and 1418 cm^{-1}.[28,32] From Figure 5, it is observed that the surface of all the unabraded films consists primarily of γ crystals as shown by the solid arrows indicating only two peaks at 1463 and 1436 cm^{-1}. The 1477 and 1418 cm^{-1} peaks due to the α crystals are barely visible as shoulders. The crystal composition of the film surface is thus similar to that of the bulk as confirmed by WAXS results. After abrasion, however, the two peaks attributed to the α phase (as indicated by the dashed arrows in Fig. 5) become much more distinct for all three samples, in addition to the γ peaks.

Figure 6 shows the ATR spectra of the unabraded and abraded surfaces of pure nylon 6 and nanocomposites containing 4 and 8 wt % MMT nanocomposites in the 900–1140 cm^{-1} region. This region contains both the CO—NH stretching peaks from the nylon 6 crystals and the Si—O stretching bands (dash-dot arrows) from clay. The three peaks from MMT clay are Si—O stretching bands at 1084, 1038, and 1010 cm^{-1}.[26,27,31,33] Before abrasion, the 976 cm^{-1} peak (solid arrow) from the γ crystal is present in all the spectra, whereas the α peak at 930 cm^{-1} can hardly be seen due to the stronger γ peak at 914 cm^{-1}.[34] After abrasion, the α peak at 930 cm^{-1} (dashed arrow) appears in all the film surfaces. There is also a corresponding decrease in the intensity of the γ peaks at 976 and 914 cm^{-1}. This confirms that α crystals were generated on the film surface during abrasion.

The ATR technique can also be utilized to shed some light on how the α crystals were created, by analyzing the peak areas of the different crystal phases on the surfaces. The 930 and 914 cm^{-1} peaks will be used to determine the amounts of the α and γ phases, respectively. Although these two peaks overlap, they can be deconvoluted quite easily as

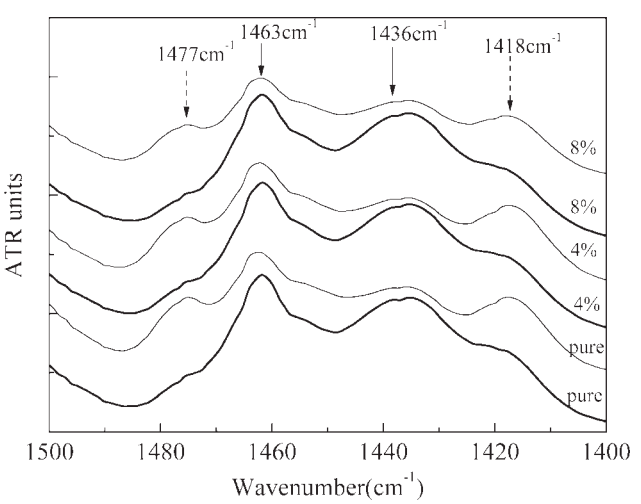

Figure 5 ATR spectra of the 1400–1500 cm^{-1} region for pure nylon 6 and nylon 6 nanocomposites containing 4 and 8 wt % MMT before (thick solid lines) and after (thin solid lines) abrasion test.

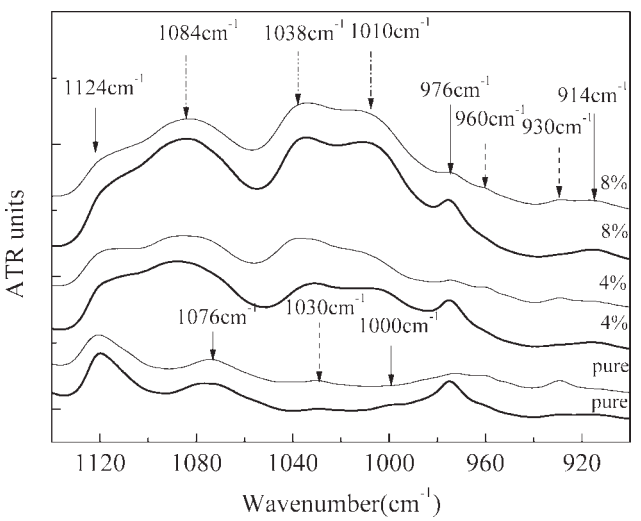

Figure 6 ATR spectra of the 900–1140 cm^{-1} region for pure nylon 6 and nylon 6 nanocomoposites containing 4 and 8 wt % MMT before (thick solid lines) and after (thin solid lines) abrasion test.

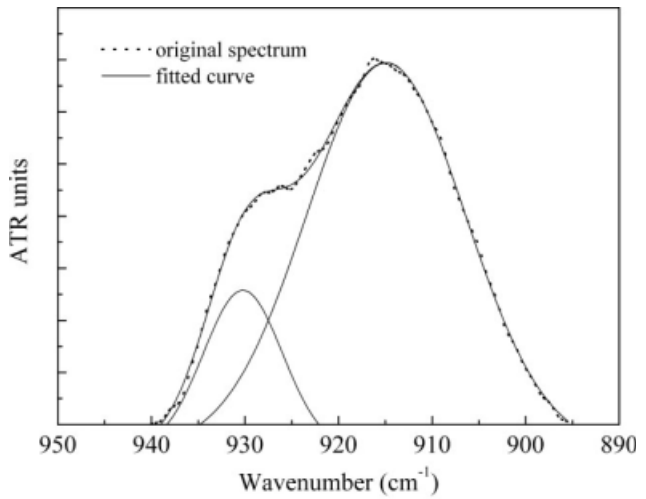

Figure 7 Example of the peak fitting procedure.

there are no other peaks in this region. Figure 7 shows an example of the peak-fitting procedure. For this analysis, the γ peak at 914 cm^{-1} is preferred over the more strongly absorbing peak at 975 cm^{-1} because the latter overlaps strongly with the clay peaks in the nanocomposites.

Figure 8 shows the peak areas A_{930} and A_{914} for the film surfaces plotted against clay content, before and after abrasion: A_{930} and A_{914} refer to the areas under the 930 and 914 cm^{-1} peaks, respectively. From Figure 8(a), it is observed that, for every sample, the value of A_{930} is much higher after abrasion compared to before abrasion. This indicates that there is an increase in the amount of α crystals on the surface as a result of the abrasion process. Furthermore, the magnitude of increase is largest for the pure nylon 6 surface, and smallest for the nanocomposite containing 8 wt % MMT. From Figure 8(b), it is seen that the value of A_{914} decreases after abrasion for all samples, implying a decrease in the amount of γ crystals on the abraded surface.

Based on these results, we propose that the α crystals on the surface were formed from the γ crystals as a result of abrasion. Specifically, this transformation is attributed to tensile forces during the abrasion process. The strain-induced γ to α crystal transition is a common phenomenon and has been observed and studied by other researchers.[25,35–38] Miyasaka and Makishima proposed that the driving force for this crystalline transformation is due to the formation of the more stable hydrogen bonds during the tensile drawing process.[39] As the γ phase crystal is 3% shorter than α phase due to the twisting of the amide group, the application of a tensile force will induce the stretching of the crystal chains. When the stretched chain length reaches that of the α crystal, a more stable hydrogen bond network between antiparallel chains is formed, resulting in the γ phase crystals being transformed into α crystals. Furthermore, strain-induced transformation of the mesomorphous β phase to the α phase has also been observed for nylon 6.[36] It is likely that some α crystals could also be formed from this transformation, but further work will be needed to prove this.

Furthermore, as clay content increases, the relative amount of α crystals on the abraded surface decreases, implying that less of the γ phase were being transformed into α crystals during abrasion. Hence, the presence of MMT renders the films less ductile, resulting in more cutting and less tensile tearing occurring during the abrasion process.

Surface composition changes observed by XPS

It is also instructive to compare the relative compositional changes of the polymer and nanofiller at the nanocomposite film surface before and after abrasion. This is achieved by using XPS technique.

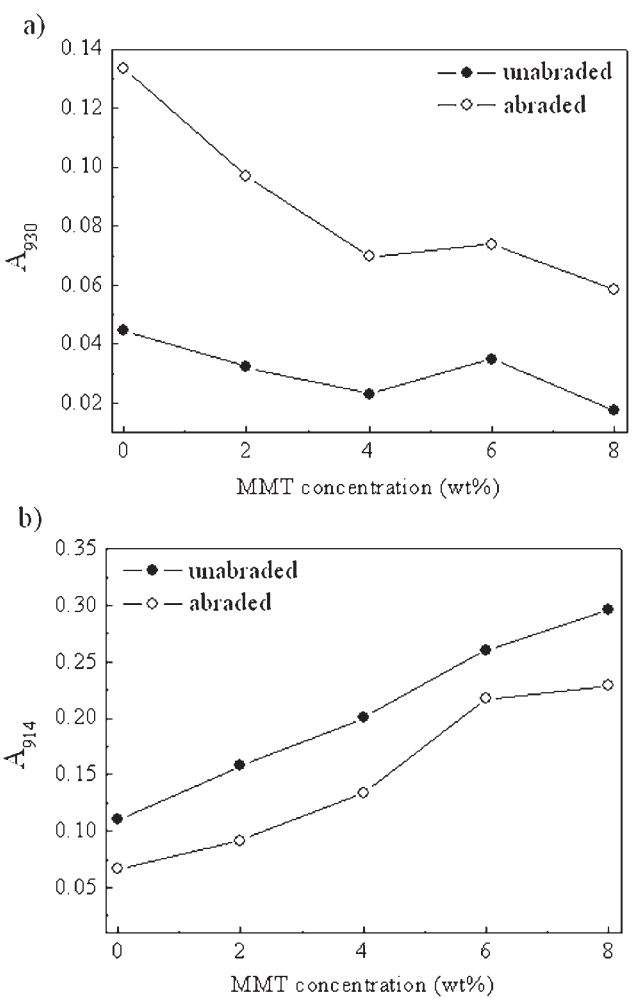

Figure 8 The peak areas (a) A_{930} and (b) A_{914} for the surfaces plotted against clay content, before and after abrasion. A_{930} and A_{914} refer to the areas under the 930 and 914 cm^{-1} peaks, respectively.

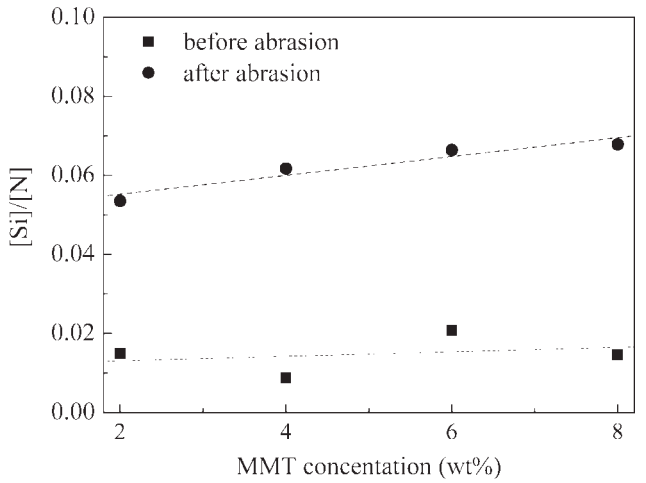

Figure 9 The element ratio of [Si]/[N] as determined by XPS before and after abrasion as a function of MMT concentration.

Figure 9 shows the XPS results of the surface composition before and after abrasion as a function of clay content. The ratio of silicon to nitrogen atoms, [Si]/[N], is used to compare the relative amount of MMT and polymer at the surface. It is observed that at every clay concentration, the value of the [Si]/[N] ratio is higher for the sample after abrasion than that before abrasion. This shows that it is easier for the polymer matrix to be removed from the surface in the presence of clay particles. As the amount of clay increases, the loss of the polymer matrix due to abrasion increases. He et al.[15] did a study on the mechanisms for the embrittlement of nylon 6/clay nanocomposites. They concluded that this embrittlement was caused by the clay dispersed in the polymer matrix, which triggered the formation of numerous crazes and microcracks near the interface between the clay and matrix. This phenomenon has been observed by transmission electron microscopy and collaborated by small-angle X-ray scanning. For the materials in our study, the presence of such defects at the clay–polymer interface would make it easier for nylon polymer to be removed from the surface during abrasion. This is why the presence of the nanoclay does not enhance the abrasion resistance of the nanocomposites but rather worsen the wear behavior. Increasing the clay content would increase the density of such defects on the surface, making the nanocomposite even more susceptible to abrasive wear. What is promising about the XPS results is that the increased amount of clay on the abraded surface would indicate that it is more difficult to remove clay from the surface compared to the polymer. Hence the MMT particles can be anticipated to impart greater abrasion resistance to the nanocomposites if one can reduce the number of defects at the matrix–particle interface.

SUMMARY AND CONCLUSIONS

Abrasion tests were performed on commercial nylon 6 and nylon 6/MMT nanocomposite films and the surfaces were analyzed by SEM, FTIR-ATR, and XPS. The following observations and conclusions can be drawn:

1. Tensile tearing is the dominant wear mechanism for all the samples. This is confirmed by both SEM and FTIR results. SEM images of all samples show fractured particles on the abraded surfaces. FTIR results indicate an increase in the amount of α crystals and a decrease in the amount of γ crystals on the surface after abrasion. This is attributed to strain-induced γ to α (and possibly β to α) transformation.
2. The cutting mechanism becomes more important when MMT content increases. SEM images show that the surface of pure nylon 6 surface is more homogeneous and has more fractured particles and less obvious grooves. However, with increasing MMT content, the damage on the surface becomes more serious and grooves become deeper. FTIR results show that the largest amount of α crystals were formed in pure nylon 6, and the amount of α crystals formed decreases with increasing MMT content.
3. The polymer matrix is easier to be removed than clay during the abrasion process. This is borne by the XPS results, which show an increase in the [Si]/[N] ratio for all the nanocomposites after abrasion.

This work has shown that it is possible to use of FTIR-ATR and XPS to investigate the micromechanics of the abrasion process, particularly for nylon nanocomposites. FTIR and XPS can be used to probe structural and compositional changes, which can be correlated to the deformation processes involved. This would allow one to design polymer nanocomposite system with better abrasion resistance. In nylon 6/MMT systems, the poor abrasion resistance is attributed to defects at the clay–polymer interface, resulting in greater wear of the polymer matrix as the content of nanofiller increases. Removing or reducing such defects, such as through modifying clay surface with suitable surfactants, would result in better performance of the nanocomposites.

The authors thank Prof. Mary Chan for providing the materials and equipment.

References

1. Lancaster, J. K. Wear 1969, 14, 223.
2. Budinski, K. G. Wear 1997, 203, 302.
3. Rajesh, J. J.; Bijwe, J.; Tewari, U. S. Wear 2002, 252, 769.

4. Bijwe, J.; Indumathi, J.; Rajesh, J. J.; Fahim, M. Wear 2001, 249, 715.
5. Shipway, P. H.; Ngao, N. K. Wear 2003, 255, 742.
6. Vaziri, M.; Spurr, R. T.; Stott, F. H. Wear 1988, 122, 329.
7. Srinath, G.; Gnanamoorthy, R. J Mater Sci 2007, 42, 8326.
8. Ratner, S. B.; Farberova, I. I.; Radyukevich, O. V.; Lure, E. G. In Abrasion of Rubber; James, D. I., Ed.; MacLaren: London, 1967; p 145.
9. Ratner, S. N.; Farberoua, I. I.; Radyukeuich, O. V.; Lure, E. G. Sov Plast 1964, 7, 37.
10. Lancaster, J. K. Plast Polym 1973, 41, 297.
11. Tian, M.; Cheng, L. J.; Liang, W. L.; Zhang, L. Q. J Appl Polym Sci 2006, 101, 2725.
12. Avella, M.; Errico, M. E.; Martuscelli, E. Nano Lett 2001, 1, 213.
13. Bauer, F.; Mehnert, R. J Polym Res 2005, 12, 483.
14. Zeng, Q. H.; Yu, A. B.; Lu, G. Q.; Paul, D. R. J Nanosci Nanotechnol 2005, 5, 1574.
15. He, C. B.; Liu, T. X.; Tjiu, W. C.; Sue, H. J.; Yee, A. F. Macromolecules 2008, 41, 193.
16. Liu, T. X.; Liu, Z. H.; Ma, K. X.; Shen, L.; Zeng, K. Y.; He, C. B. Compos Sci Technol 2003, 63, 331.
17. Srinath, G.; Gnanamoorthy, R. Mater Sci Eng A 2006, 435, 181.
18. Celini, N.; Bergaya, F.; Poncin-Epaillard, F. Polymer 2007, 48, 58.
19. Loo, L. S.; Gleason, K. K. Macromolecules 2003, 36, 2587.
20. Samyn, P.; Schoukens, G.; Verpoort, F.; Van Craenenbroeck, J.; De Baets, P. Macromol Mater Eng 2007, 292, 523.
21. De Jaeger, R.; Mazzah, A.; Gengembre, L.; Frere, M.; Jama, C.; Milani, R.; Bertani, R.; Gleria, M. J Appl Polym Sci 2008, 108, 3191.
22. Park, S. Y.; Cho, Y. H.; Vaia, R. A. Macromolecules 2005, 38, 1729.
23. Murthy, N. S. J Polym Sci Part B: Polym Phys 2006, 44, 1763.
24. Holmes, R.; Bunn, D. W.; Smith, D. L. J Polym Sci 1955, 17, 619.
25. Arimoto, H.; Ishibashi, M.; Hirai, M. J Polym Sci Part A: Gen Pap 1965, 3, 317.
26. Loo, L. S.; Gleason, K. K. Polymer 2004, 45, 5933.
27. Cole, K. C.; Depecker, C.; Jutigny, M.; Lefebvre, J. M.; Krawczak, P. Polym Eng Sci 2004, 44, 231.
28. Bureau, M. N.; Denault, J.; Cole, K. C.; Enright, G. D. Polym Eng Sci 2002, 42, 1897.
29. Arimoto, H. J Polym Sci Part A: Gen Pap 1964, 2, 2283.
30. Schneider, B.; Schmidt, P.; Wichterle, O. Coll Czech Chem Commun 1962, 27, 1749.
31. Vasanthan, N.; Salem, D. R. J Polym Sci Part B: Polym Phys 2001, 39, 536.
32. Chen, C.; Swenson, C. A. J Phys Chem 1969, 73, 2999.
33. Farmer, V. C.; Russell, J. D. Spectrochim Acta 1963, 20, 1149.
34. Rotter, G.; Ishida, H. J Polym Sci Part B: Polym Phys 1992, 30, 489.
35. Miyasaka, K.; Makishima, K. J Polym Sci Part A-1: Polym Chem 1968, 6, 1317.
36. Penel-Pierron, L.; Seguela, R.; Lefebvre, J. M.; Miri, V.; Depecker, C.; Jutigny, M.; Pabiot, J. J Polym Sci Part B: Polym Phys 2001, 39, 1224.
37. Ito, M.; Takahashi, A.; Araki, N.; Kanamoto, T. Polymer 2001, 42, 241.
38. Dencheva, N.; Denchev, Z.; Oliveira, M. J.; Funari, S. S. J Appl Polym Sci 2007, 103, 2242.
39. Miyasaka, K.; Makishima, K. J Polym Sci Part A-1: Polym Chem 1967, 5, 3017.